Supplement of Geosci. Model Dev., 16, 6211–6245, 2023
https://doi.org/10.5194/gmd-16-6211-2023-supplement

Geoscientific Model Development
Open Access
EGU

Supplement of

Overcoming computational challenges to realize meter- to submeter-scale resolution in cloud simulations using the super-droplet method

Toshiki Matsushima et al.

Correspondence to: Toshiki Matsushima (toshiki@gfd-dennou.org)

S1 The impact of the numerical accuracy of the CVI scheme

We performed additional experiments to investigate the impact of the numerical accuracy of the CVI scheme on the time evolution of the tracer fields. These were modifications of the warm bubble experiments described in our manuscript. The domain size for these experiments is $300\,\mathrm{m} \times 8{,}000\,\mathrm{m} \times 5{,}000\,\mathrm{m}$ for x, y, and z directions. The spatial resolution is $100\,\mathrm{m} \times 500\,\mathrm{m} \times 500\,\mathrm{m}$. We introduced a prescribed two-dimensional Benard-convection-like flow in which the cell positions oscillate periodically. The density and the mass stream function are represented as follows:

$$\rho_0 = 1\,[\mathrm{kg \cdot m^{-3}}], \tag{S1}$$

$$\psi(y,z,t) = \frac{50{,}000}{\pi} \sin\left(\frac{\pi z}{5{,}000\,\mathrm{m}}\right)\left[\sin\left(\frac{2\pi y}{8{,}000\,\mathrm{m}}\right) + \epsilon \cos\left(\frac{2\pi y}{8{,}000\,\mathrm{m}}\right)\cos\left(\frac{2\pi t}{1{,}800\,\mathrm{s}}\right)\right]\,[\mathrm{kg \cdot m^{-1} s^{-1}}], \tag{S2}$$

$$\rho_0 v(y,z,t) = -\frac{\partial \psi}{\partial z}\,[\mathrm{m \cdot s^{-1}}], \tag{S3}$$

$$\rho_0 w(y,z,t) = \frac{\partial \psi}{\partial y}\,[\mathrm{m \cdot s^{-1}}]. \tag{S4}$$

Here, $\epsilon = 0.5$. Even for such a simple 2D flow, the time evolution of particles can be chaotic because the flow is unsteady (Malhotra et al. 1998). The momentum fields and the mass stream function at the initial time ($t = 0\,\mathrm{min}$) are shown in Fig. S1. The vorticity of the flow is given by

$$\zeta = -\left[\left(\frac{\pi}{5{,}000\,\mathrm{m}}\right)^2 + \left(\frac{2\pi}{8{,}000\,\mathrm{m}}\right)^2\right]\psi(y,z,t). \tag{S5}$$

As described in our manuscript, the CVI-1 cannot incorporate the effect of shear and vortical flow within a cell to the SD movement, but CVI-2 can. Thus, the prescribed flow serves as a case in which the effects of the numerical accuracy in the CVI are likely to be verified.

First, we investigate the time evolutions of the particle distributions. An average of 3,200 particles per cell (128 for $100^3\,\mathrm{m}^3$ volume) was initially distributed in 3D space quasi-uniformly (Sobol sequences). The time integrations of particle positions using the CVI-1, CVI-2, and analytical expression of velocities were performed for $21{,}600\,\mathrm{s}$ by $\Delta t = 1.0\,\mathrm{s}$. The time evolutions of particle distributions are shown in Fig. S2. When the CVI-1 is used, a staircase-like pattern appears, and the particles mix well, especially at the central positions of the vorticities centered around $y = 1{,}500\,\mathrm{m}$ and $y = 5{,}500\,\mathrm{m}$. In contrast, such patterns are not present in CVI-2 and ANL; Instead, small and thin filaments are depicted in CVI-2 and ANL. In our original manuscript, we could not compare the particle distributions obtained by CVI-1 and CVI-2 to the reference solution. However, our latest results confirm that switching from CVI-1 to CVI-2 improves particle distributions, aligning them more closely with the reference solution.

Now, we address how the numerical accuracy of particle distributions affects that of the tracer distributions (i.e., the statistics over the grid fields). In our calculations, we can track each particle's ID (or initial position of particles), enabling us to monitor the time evolutions of tracer fields for arbitrary initial tracer fields without the need to recalculate the time evolutions of the particle distributions. The initial conditions of the tracer field ϕ are defined as follows.

$$\phi(y,z,t=0) = \sin\left(\frac{\pi k z}{5{,}000\,\mathrm{m}}\right)\left[\sin\left(\frac{2\pi l y}{8{,}000\,\mathrm{m}}\right) + \epsilon \cos\left(\frac{2\pi l y}{8{,}000\,\mathrm{m}}\right)\right] + \sqrt{1+\epsilon^2} \tag{S6}$$

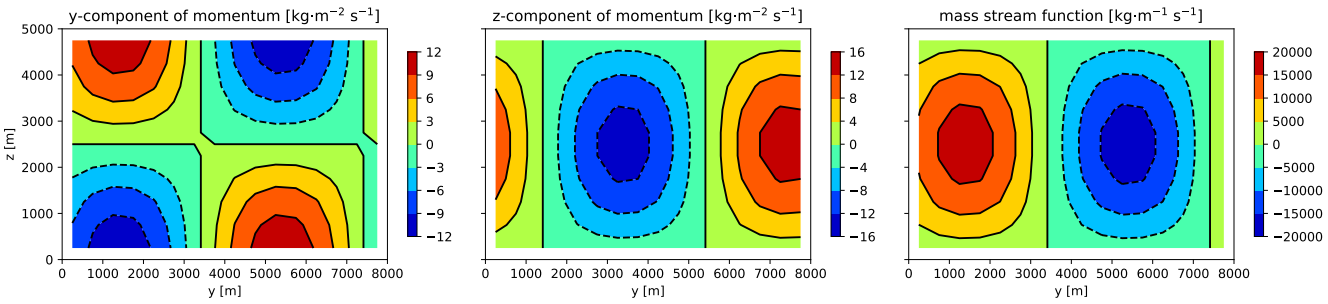

Figure S1. The momentum fields and the mass stream function at the initial time.

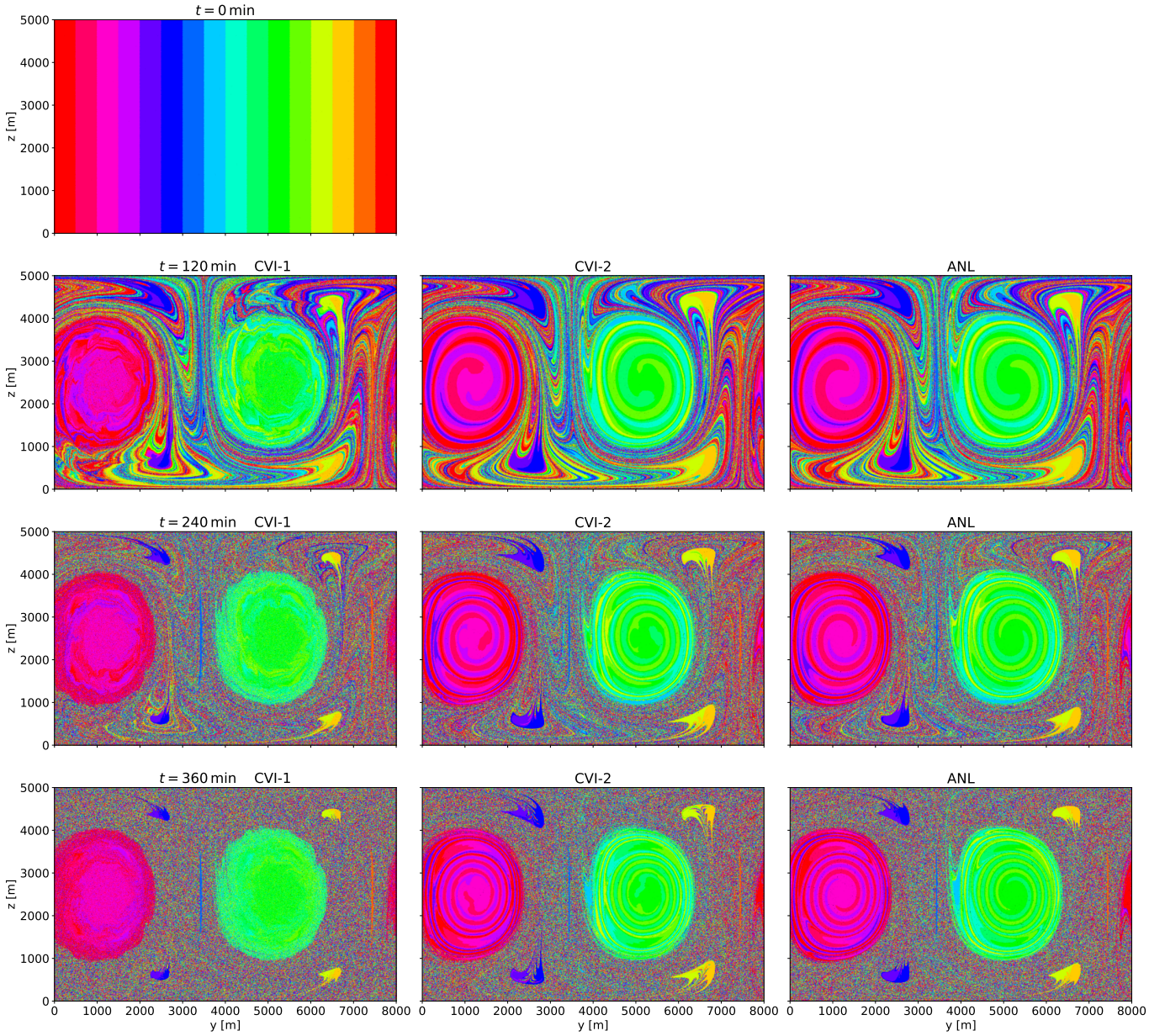

Figure S2. Distributions of particle positions colored by the initial y coordinate (Y) when CVI-1, CVI-2, and analytical velocities are used for particle movement.

We construct the initial tracer fields by scaling and shifting the stream function described in Eq. (S2) to ensure $\phi \geq 0$. Additionally, we introduce wavenumber parameters (k, l) to control the spatial scale of the initial distributions. Instead of sampling particles to ensure consistency between the particle number density and tracer concentration, we sample numerous particles quasi-uniformly across the computational domain. We then assign a multiplicity to each particle, allowing us to manage tracer distribution time evolutions more efficiently. We examine the time evolution of the tracer fields for the initial distributions with the wavenumbers $(k, l) = (1, 1), (4, 3)$, and $(8, 5)$. The error is quantified as the L^2 norm of the difference between the tracer fields obtained using CVI-1 or CVI-2 and analytical velocities. These time evolutions of the errors are shown in Fig. S3. Note that the time evolutions of the tracer fields can be found in the appendix of this letter. In all cases, the errors when using CVI-2 are reduced compared to CVI-1, especially during the time $t < 180$ min. The numerical accuracy of the CVI scheme has a more significant impact on the errors as the wavenumbers increase. The errors grow over time when $(k, l) = (1, 1)$, and the differences between CVI-1 and CVI-2 become statistically indistinguishable. However, CVI-2 still manages to reduce the errors even during extended simulated time, and the statistical differences between CVI-1 and CVI-2 remain apparent when $(k, l) = (8, 5)$.

These results provide insights into the effect of the numerical accuracy of the CVI scheme on cloud simulations.

- The particle distributions and transient time evolutions of the tracer fields are significantly improved in alignment with the

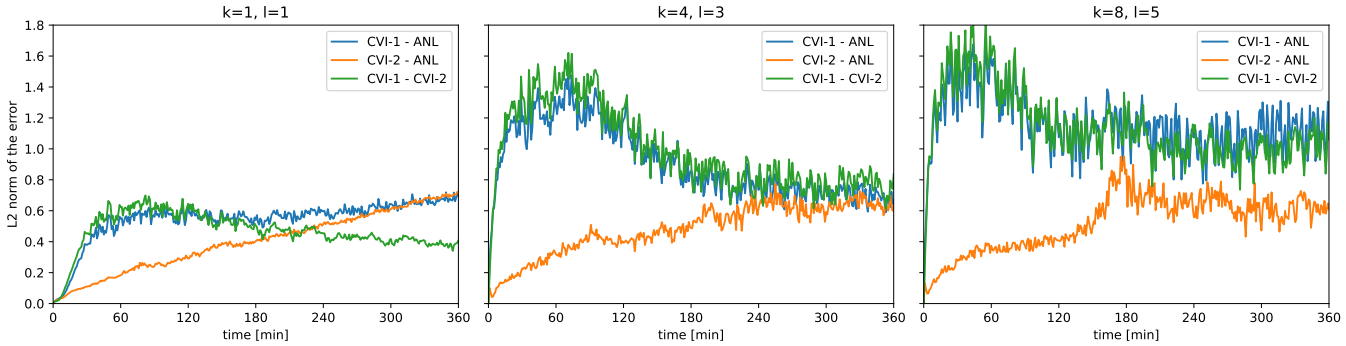

Figure S3. The time evolutions of the errors between the tracer fields obtained using CVI-1 or CVI-2 and analytical velocities for each initial tracer distribution with the wavenumbers $(k, l) = (1, 1), (4, 3)$, and $(8, 5)$.

reference solution when using the CVI-2 scheme instead of CVI-1.

- The impact of the CVI's numerical accuracy on errors is minimal for large-scale initial distributions. Since small-scale fluctuations of the DSD cannot be represented at the spatial resolutions often used in LES, it might be challenging to verify the CVI-2 scheme's impact on whole-cloud structures.
- In contrast, the effect of the CVI scheme's numerical accuracy is evident for small-scale tracer distributions. Although particle-based advection avoids numerical diffusion for each particle's information due to its algorithms, the CVI-1's effect might manifest as macroscopic and spurious numerical diffusion.
- If this occurs in meter-to-submeter scale cloud simulations, we might detect a statistical difference in the LWC between CVI-1 and CVI-2, as the LWC fluctuates due to small-scale turbulence mixing. This detection is analogous to how we discern the numerical accuracy of advection schemes through differences in effective resolution.
- The statistical difference in small-scale tracer fields might indirectly affect large-scale cloud fields through interactions between the eddies and microphysics.

S2 Differences in LWC across model versions and improvements

To investigate the contribution of the model version and improvement, we performed warm bubble experiments by taking as many SDs as possible (SD32768). Figure S4 shows the LWC for different model versions and settings. The upper right panel in Fig. S4 shows the LWC obtained with SDM-new, using almost the same setup as for SDM-orig, except for some minor modifications (numerical representation precision, random number seeds, order of calculations, etc.). Then, we considered model improvements (lower left panel in Fig. S4), including the exclusion of the monotone FCT, the use of time-averaged variables during each long time step for the calculations of microphysics, the use of CVI-2, the use SDs sampling from PDF, which is proportional to total density, and the use of Sobol sequence for initialization. Lastly, we simplified the model setup by reducing collision–coalescence calculations in noncloudy cells and ignoring pressure dependence on coefficient A for condensation calculations (the lower right panel in Fig. S4). The difference in the upper left and right panels is very small, indicating consistency between SDM-orig and SDM-new. The model improvement in this study resulted in slightly different results for precipitation timing and behavior of clouds in the upper layer. The simplification of the calculations resulted in a small difference in LWC.

Based on the above discussion, we conclude that the model version is unimportant and the difference in the results between SDM-orig and SDM-new becomes smaller for many SDs, indicating that sampling and randomness caused the differences.

References

Malhotra, N., Mezić, I., and Wiggins, S.: Patchiness: A new diagnostic for Lagrangian trajectory analysis in time-dependent fluid flows, Int. J. Bifurc. Chaos Appl. Sci. Eng., 8, 1053–1093, doi:10.1142/S0218127498000875, 1998.

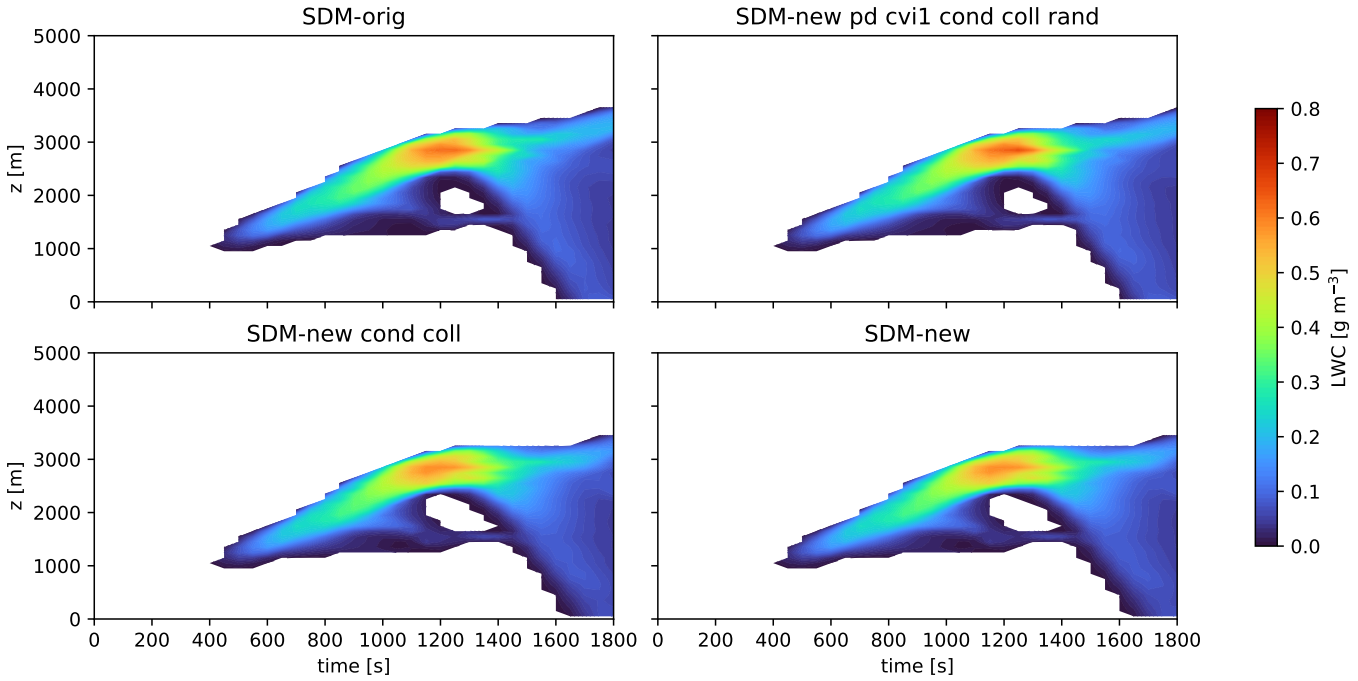

Figure S4. Horizontally averaged time-height cross-section of the liquid water content (LWC) for SDM-orig32768 and SDM-new32768 using different settings. Note that only regions with LWC higher than $0.001\,\mathrm{g}\cdot\mathrm{m}^{-3}$ are shown.

Appendix: time evolutions of the tracer distributions and the L^2 norm errors

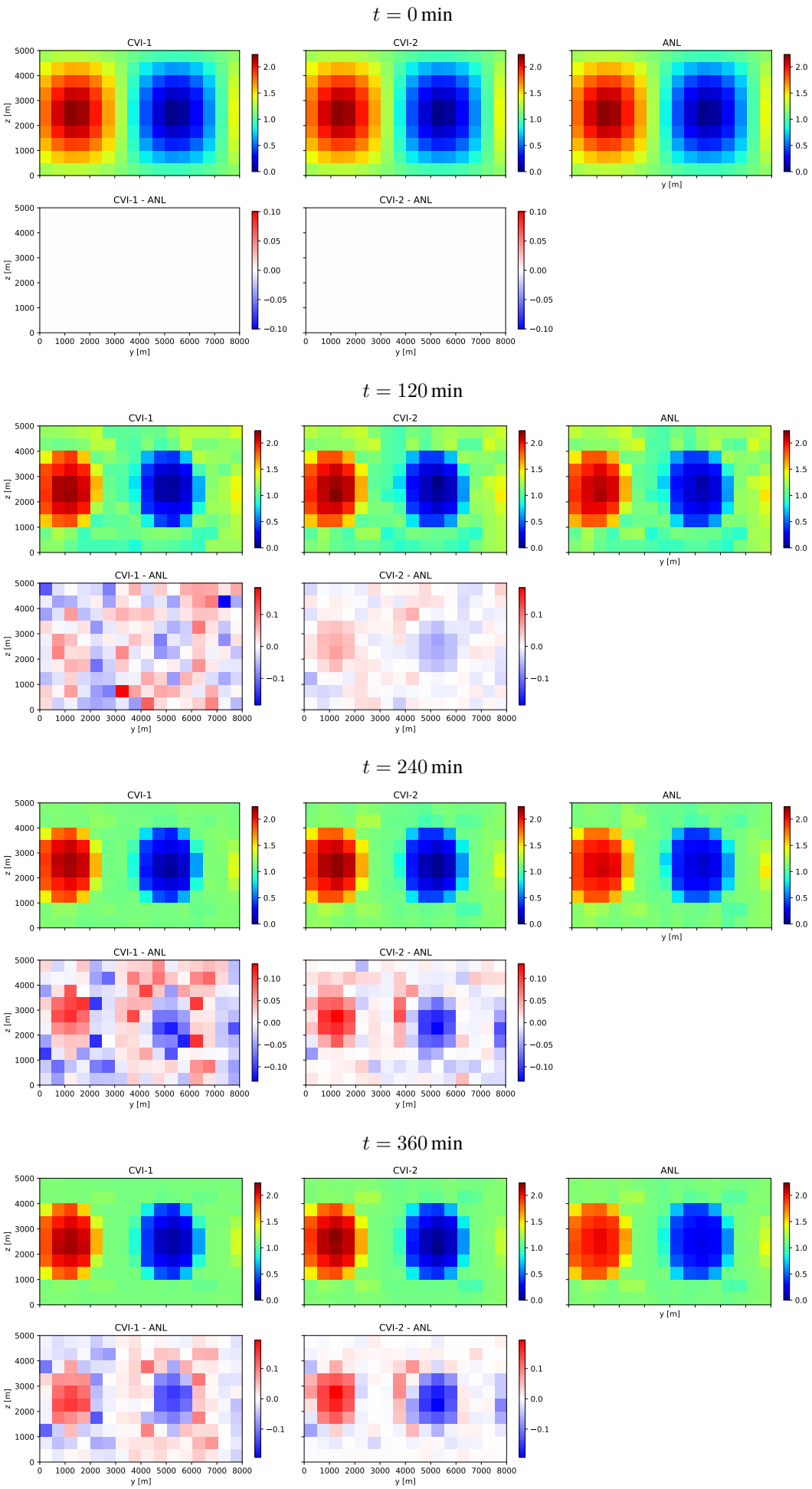

Figure S5. The case for initial tracer distributions with wavenumbers $(k, l) = (1, 1)$

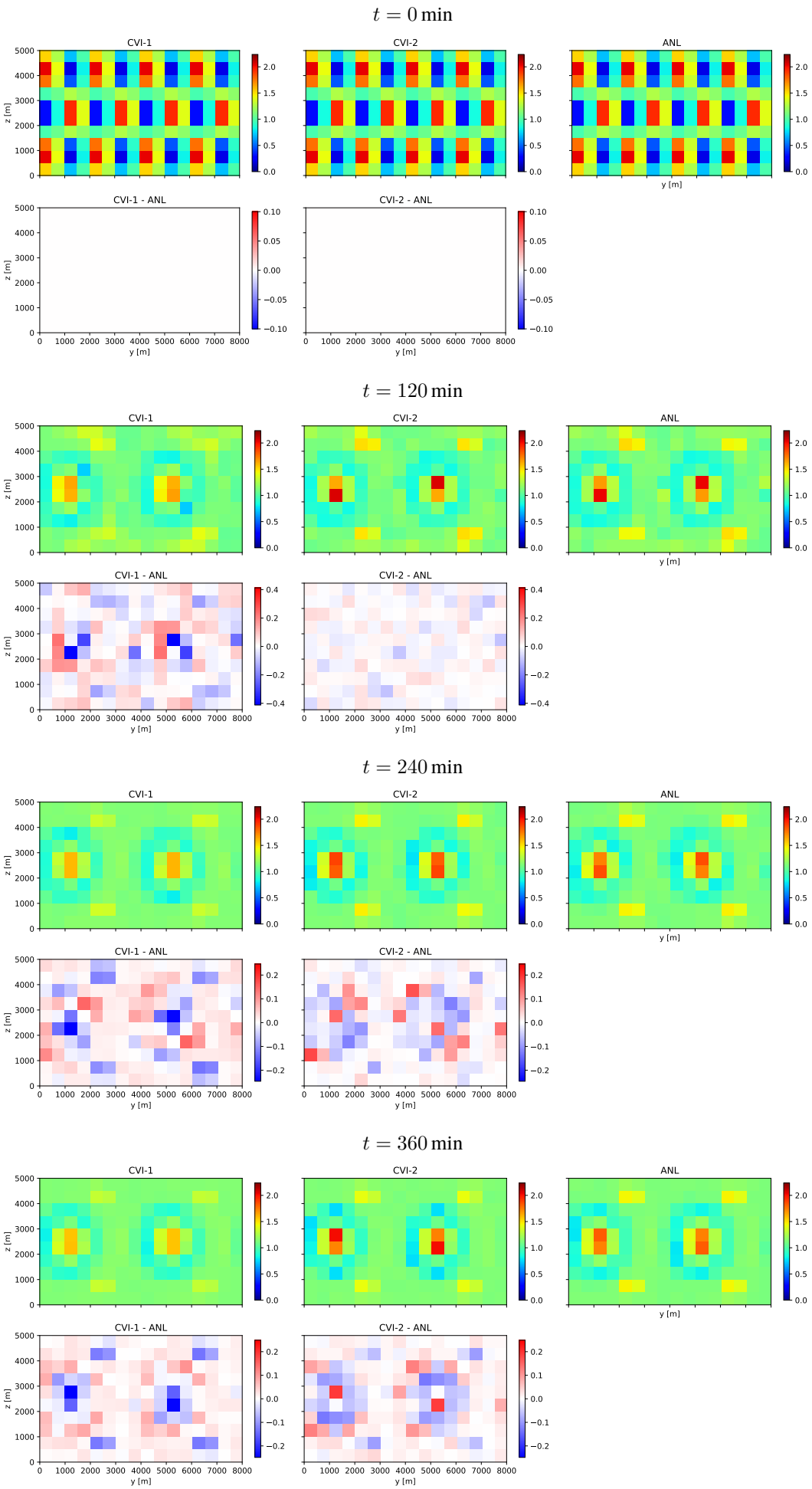

Figure S6. The case for initial tracer distributions with wavenumbers $(k, l) = (4, 3)$

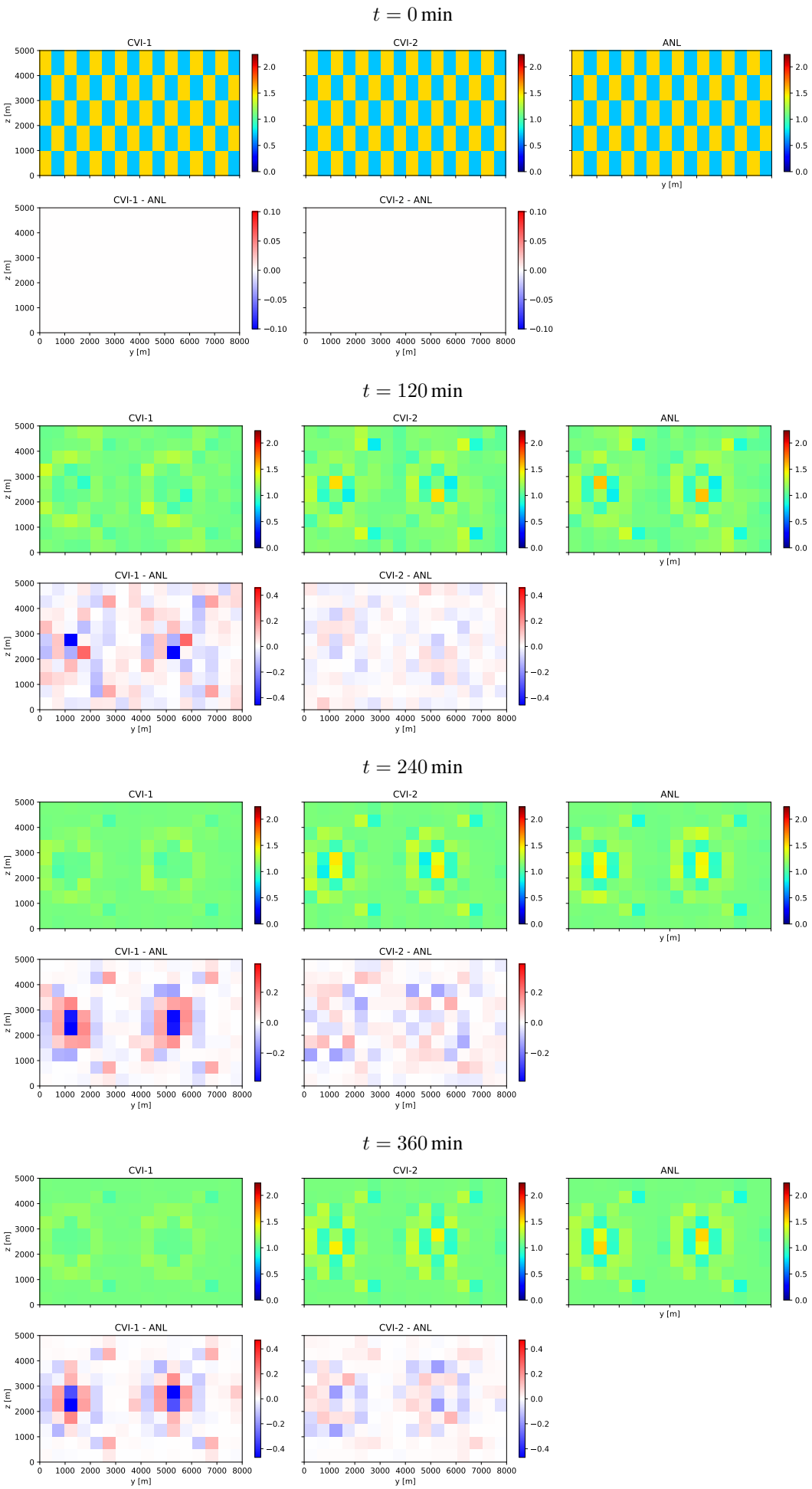

Figure S7. The case for initial tracer distributions with wavenumbers $(k, l) = (8, 5)$